

# Pressure and velocity fluctuations in the atmospheric boundary layer

M. Sterling<sup>†</sup> and C. J. Baker<sup>‡</sup>

*School of Engineering, The University of Birmingham, Edgbaston, Birmingham, B15 2TT, UK*

A. D. Quinn<sup>‡†</sup> and R. P. Hoxey<sup>‡‡</sup>

*Silsoe Research Institute, Wrest Park, Silsoe, Bedford, MK45 4HS, UK*

*(Received April 19, 2004, Accepted December 2, 2004)*

**Abstract.** This paper presents an analysis of wind velocity and pressure data obtained in a rural environment with a view to identifying the vortex structures present within the flow and examining the relationship between pressure and dynamic pressure. The data is analysed using both conventional analysis and conditional sampling. A method examining the eigenvalues of a matrix formed by the addition of the square of the strain tensor and the square of the vorticity tensor is also investigated. This method illustrates that there are a number of vortex structures present in the flow. The work presented in this paper suggests that the extreme events occur as a result of the superposition of two independent mechanisms.

**Keywords:** vortex; vorticity; flow structures; conditional sampling; pressure fluctuations.

---

## 1. Introduction

It is generally accepted that coherent structures are present in the wind and in some cases dominate the overall physics of the flow, e.g., the flow over natural plant canopies are governed by such motions (see Raupach, *et al.* 1996 and Sadani and Kulkarni 2000 for detailed explanations). Despite this acceptance, agreement over what constitutes a coherent structure remains elusive. This is not surprising since it has been shown that different structures exist in different types of flow. For example, numerous references to horseshoe vortices, hairpin eddies, pancake eddies, surfboard eddies, vortex rings and mushroom eddies can be found in the literature (Fiedler 1988). In addition a significant amount of research has been undertaken trying to elucidate the structure of the intermittent organised motion that occurs in boundary layer flow. Numerous research articles have been written on this subject (Robinson 1991, Sadani and Kulkarni 2000) as well the pioneering work by Hussain and his co-workers (Hussain 1983, Hussain 1986 and Jeong and Hussain 1995 to

---

<sup>†</sup> Lecturer, Corresponding Author, E-mail: [m.sterling@bham.ac.uk](mailto:m.sterling@bham.ac.uk)

<sup>‡</sup> Professor

<sup>‡†</sup> Senior Research Scientist

<sup>‡‡</sup> Head of Research Group

cite but a few examples). To the best of the authors knowledge, apart from an overall acceptance that such structures exist, little is known about the impact of these structures on engineering design. It has been demonstrated that high energy, small-scale events occur over a low-rise building in natural wind and that these structures may have important design implications particularly for cladding elements (Baker 2001, Sterling, *et al.* 2003). However, the shape, structure, orientation and size of these events in a natural wind have yet to be identified.

The aim of this paper is to try and identify what vortex structures exist in the wind and to investigate if these events are of particular importance to the wind engineering community. As stated by Jeong and Hussain (1995) the evolution of coherent structures and their interactions with background turbulence is governed by vortex dynamics. Hence, through an analysis of the vortex structures in the wind it is hoped that further progress can be made on identifying and monitoring the evolution of coherent structures in the lower part of the atmospheric boundary layer.

One of the main problems with identifying a vortex is associated with the frame of reference that is adopted. This can easily be illustrated by considering the streamlines associated with a simple vortex flow. It can be shown that for an ideal fluid the stream function ( $\psi$ ) for a clockwise vortex, in a Cartesian coordinate system, in the  $xy$  plane is given by:

$$\psi = -\frac{\Gamma}{2\pi} \ln \left( \sqrt{\frac{x^2 + y^2}{r_0}} \right) \quad (1)$$

(see Massey 1990), where  $\Gamma$  represents the circulation and  $r_0$  is a constant which represents the radius at which the stream function is zero. Assuming this vortex is convected by a mean flow of velocity  $U$  and that the stream function of this mean flow is given by  $-Uy$ , then the stream function of the flow can be found by superposition, i.e.:

$$\psi = -Uy - \frac{\Gamma}{2\pi} \ln \left( \sqrt{\frac{x^2 + y^2}{r_0}} \right) \quad (2)$$

Fig. 1, illustrates four values of stream functions for various values of  $U$ . When the mean velocity is zero the vortex is readily identifiable. As the mean velocity increases to 1 m/s it is still possible to recognize the vortex, however this is largely dependent on the value of stream function adopted. When the mean velocity is 10 m/s the imprint left by the vortex is that of a small peak in the lower two contours. If only the upper two contours had been selected then the presence of the vortex would pass undetected. This example is highly simplified and considers an ideal fluid, however, it

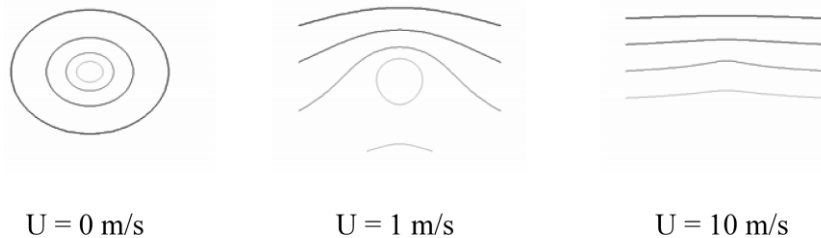


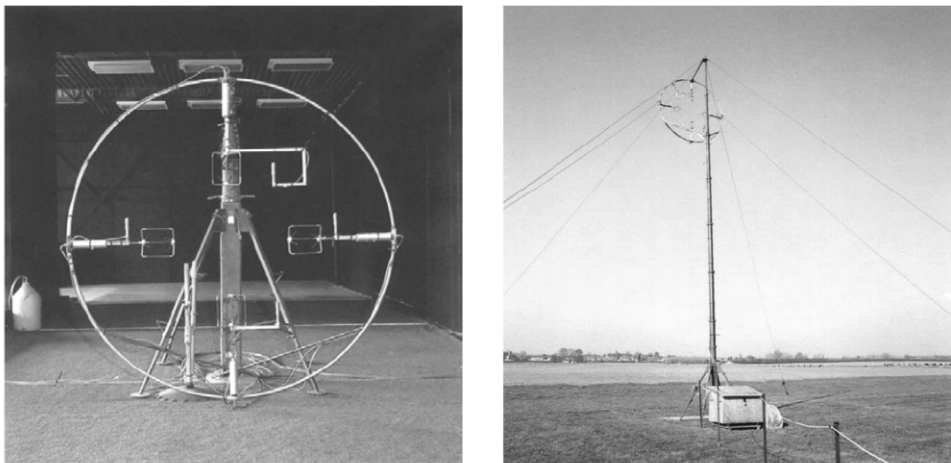
Fig. 1 Contours of  $\psi$  obtained from Eq. (2), ( $\Gamma = 1 \text{ m}^2/\text{s}$  and  $r_0 = 1 \text{ m}$ )

serves to demonstrate a point, namely the complexity of vortex identification. When real fluids with high levels of shear are considered the level of complexity is increased further.

It will be shown that despite the identification problems mentioned above it is possible to make progress and elucidate some information on vortex structure from real wind velocity and pressure data. This data was obtained from a series of experiments, full details of which are presented in Section 2. Section 3 of the paper is concerned with the conventional analysis of the experimental data, for example the calculation of first and second order statistics and spectra etc. Section 4 is devoted to the conditional analysis of the velocity and pressure data. A method proposed by Jeong and Hussain (1995) to identified vortex structures is explained and implemented in Section 5. Finally, Section 6 discusses the finding of the paper and presents some concluding remarks.

## 2. Experimental setup

The experiments were undertaken in natural wind conditions at the Silsoe Research Institute, Bedford, UK. The experimental rig was located in open country with a logarithmic velocity profile with a roughness length ( $z_0$ ) of around 0.01 m and a power law exponent of 0.15 (Richardson, *et al.* 1995). Further details of the spectral characteristics of the flow are given in Richards, *et al.* (1997). The experimental rig consisted of an approximately 2.3 m diameter ring mounted on a 15 m high pneumatic mast, (see Fig. 2(a) and 2(b)). When in operation the ring is offset from the mast by approximately 1 m. Attached to the ring were four 10 Hz sonic anemometers and four corresponding static pressure probes. The pressure probes were positioned in such a way as to be as close as possible to the anemometers without causing interference to the flow. Anemometers 1 and 4 were positioned at the bottom and top of the ring respectively, while the remaining anemometers were positioned 90 degrees from the top and bottom anemometers, pointing into the ring and in the same plane. Looking downwind, anemometers 2 and 3 are located on the left and right of



(a) Sonic anemometer 1 at base on the ring. (b) Ring offset from mast approximately 1m.

Fig. 2 Photographs illustrating the experimental rig (a) in the laboratory and (b) deployed in test conditions

Table 1 Vertical and horizontal separation (m) of anemometers and pressure probes

	Anemometers	Pressure probes
Horizontal	1.000+-0.01	1.450+-0.01
Vertical	1.000+-0.01	1.000+-0.01

anemometer 1 (see Fig. 2(a)). The same numbering applies to all of the static pressure probes. In addition, a static pressure tapping is placed beneath the rig. All of the anemometers, static probes and the ground tapping were sampled simultaneously at a rate of 10 Hz. Unfortunately, there is evidence to suggest that ground tapping was susceptible to a long-term drift, hence in what follows this tapping has only been used to calibrate the static probes. Since these calibrations occurred over a short time scale (120s) it was considered that the effect of the drift over this period was sufficiently small to be safely ignored.

The horizontal and vertical separation of the sonic anemometers and static pressure probes are given in Table 1. From the 10/04/02 to 14/05/02 a variety of experiments were undertaken. In all cases the centre of the mast was positioned 10m off the ground. As a result of the varying wind direction a significant amount of data has been collected for a variety of angles of attack. However, for the purposes of this paper attention is restricted to wind data approximately normal to the ring. This results in two datasets obtained on 29/04/02 and 14/05/02 both of which are 30 minutes in length and contain 18000 data points. A full statistical description of the data is presented in the following section.

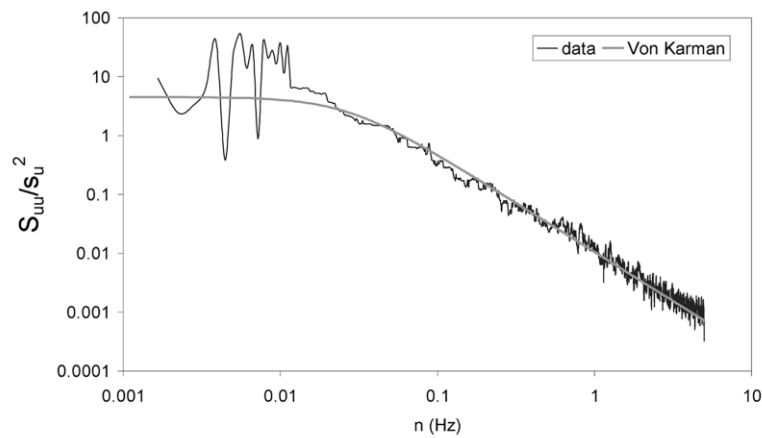
### 3. Conventional data analysis

Table 2 gives the mean wind velocity in the downwind direction  $U$ , the three turbulence intensity

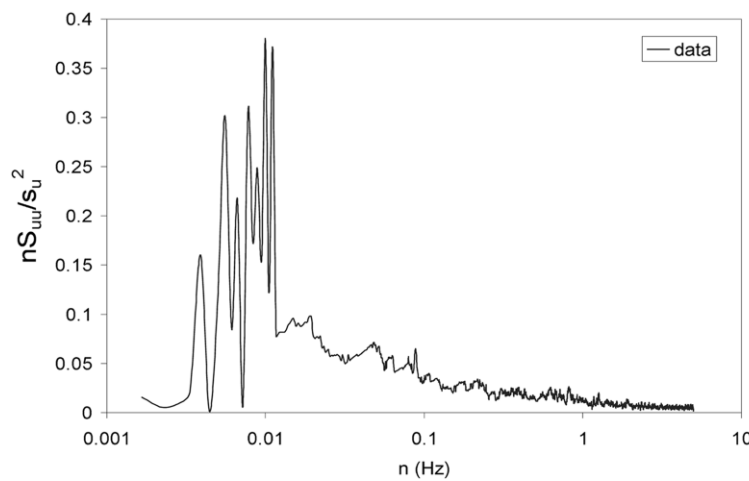
Table 2 Conventional statistical analysis of experimental velocity data

	29/04/02				14/05/02			
	1	2	3	4	1	2	3	4
$U$ (m/s)	9.821	9.802	9.722	9.852	7.259	7.350	7.272	7.414
$I_u$	0.201	0.203	0.200	0.200	0.207	0.204	0.204	0.202
$I_v$	0.178	0.164	0.161	0.179	0.164	0.141	0.143	0.158
$I_w$	0.081	0.094	0.096	0.084	0.079	0.089	0.091	0.082
Skew $u$	0.301	0.311	0.300	0.298	0.216	0.228	0.206	0.196
$U_e/U$	1.766	1.786	1.771	1.756	1.610	1.661	1.618	1.601
$u_\tau/U$	0.062	0.078	0.077	0.067	0.061	0.066	0.070	0.062
${}^xL_u$ (m)		190 (50) [170]				78 (33) [103]		
${}^xL_v$ (m)		95 (35) [148]				49 (17) [77]		
${}^xL_w$ (m)		12 (6) [3]				8 (4) [26]		
${}^yL_u$ (m)		128				102		
${}^yL_v$ (m)		96				38		
${}^yL_w$ (m)		6				12		
${}^zL_u$ (m)		152				103		
${}^zL_v$ (m)		164				32		
${}^zL_w$ (m)		5				8		

components  $\sigma_u/U$ ,  $\sigma_v/U$  and  $\sigma_w/U$ , the skewness of the  $u$  velocity components (Skew) and the ratio of the extreme wind velocity to the mean wind velocity,  $U_e/U$ . This extreme wind velocity is the 99.95<sup>th</sup> percentile and corresponds to 0.9 seconds of the dataset. The dimensionless friction velocity is represented by  $u_\tau/U$ . The  $u$  component is parallel to the mean flow direction, the  $v$  component is horizontal and perpendicular to the mean flow direction, and the  $w$  component is in the vertical direction. The remaining nine rows in Table 2 represent various lengths scales which have predominately been obtained from correlation analysis and will be discussed in more detail in the following paragraph. The columns numbered 1 to 4 in Table 2 represent the sonic anemometer number specified in the previous section.



(a)



(b)

Fig. 3 (a) An example of fitting the von Karman spectrum to the velocity data for sonic 1, 14/05/02 data (b) An example of plotting the velocity data for sonic 1, 14/05/02 in an alternative form to obtain the frequency at which  $nS_{uu}/\sigma^2$  attains a maximum

For each respective datasets there is little variation in either of the values of mean velocity or the turbulence intensities across the all the anemometers. This is to be expected given the small spacing between the anemometers, however a small increase in  $U$  and decrease in  $I_u$  can be observed between anemometers 1 and 4. The values of these parameters and that of the friction velocity are consistent with values that would be expected over rural terrain (ESDU 1985). The values of skewness are of similar orders of magnitude and illustrate a slight positive bias. The ratio of extreme to mean velocity is of the order of 1.6–1.7 and is consistent with earlier analysis of wind velocity over the experimental site (Sterling, *et al.* 2003). The values of length scales in the  $x$  direction ( ${}^xL_u$ ,  ${}^xL_v$ ,  ${}^xL_w$ ), were obtained using three approaches. The first approach is concerned with integrating the respective auto correlation functions and invoking Taylor's frozen turbulence hypothesis, while the remaining two methods assume that the von Karman spectral equations are valid (ESDU 1985). The statistics in (brackets) are calculated from the values of  $S_{ii}/\sigma_i^2$  as  $n$  tends to zero, (since  $S_{ii}/\sigma_i^2 \rightarrow 4{}^xL_i/U$  as  $n \rightarrow 0$ ), while the statistics in [brackets] are obtained from plotting the data in  $nS_{ii}/\sigma_i^2$  form and obtaining the frequencies which corresponds to the maxima (since at  $S_{uu}/\sigma_u^2_{\max}$ ,  $n{}^xL_u/U = 0.146$  and  $S_{ii}/\sigma_i^2_{\max}$ ,  $n{}^xL_i/U = 0.106$ ,  $i = v$  and  $w$ ). This approach is shown graphically in Figs. 3(a) and 3(b). Only one value is shown for all the anemometers in a specific dataset since the degree of difference between different anemometers using the same method to obtain the required length scale was negligible. However, these length scales differ widely depending on the method of calculation. This is a trend that has also been reported elsewhere and is partly attributed to the inability of the von Karman model to adequately represent turbulence characteristics at all frequencies (ESDU 1985). The large differences between the latter two methods, which use the same equations, suggest that the first approach using the autocorrelation function is more appropriate. However, this method is also prone to errors since in practise the integration of the appropriate correlation function is not performed until infinity but instead until the first zero crossing of the function with the time axis. Hence, it is possible for low values of autocorrelation with large time lags to significantly influence the final calculation. When such an instance occurred the correlation function was integrated until the slope of the function approached zero. The remaining six lengths scales were obtained by integrating the cross correlation function obtained from the appropriate velocity components of the required anemometer. For example, for  ${}^zL_v$  the cross correlation function was found from the  $v$  component of anemometer 1 and the  $v$  component of anemometer 4. These remaining length scales are of a similar order of magnitude across both datasets with the exception of  ${}^yL_v$  and  ${}^zL_v$ . Notwithstanding these differences in length scales, the data are broadly consistent and of similar magnitudes to enable detailed analysis to be undertaken with confidence in the applicability of the results.

Fig. 4(a) illustrates a typical probability distribution for the three velocity components of anemometer 1;  $u'$ ,  $v'$  and  $w'$  represents the fluctuating velocity components in the  $x$ ,  $y$  and  $z$  directions respectively. Subsequent analysis of all anemometers for both datasets confirms the results of Fig. 4(a), i.e., all the velocity components follow a Gaussian distribution. The values of skewness given in Table 2 do not appear to be replicated in Fig. 4(a). This is mainly due to a number of relatively large fluctuations at the extremity of the distributions influencing the overall calculation. The effect of these large values can be seen in Fig. 4(b) which illustrates a deviation from Gaussian at the tails of the distribution.

Fig. 5 illustrates the power spectra for all three velocity components. The spectral density for each component ( $S_{uu}$ ,  $S_{vv}$ ,  $S_{ww}$ ) is divided by its variance ( $\sigma_u^2$ ,  $\sigma_v^2$ ,  $\sigma_w^2$ ) and plotted against frequency  $n$ . The inertial sub range is clearly seen at higher frequencies ( $n > 0.3$  Hz) for all three components,

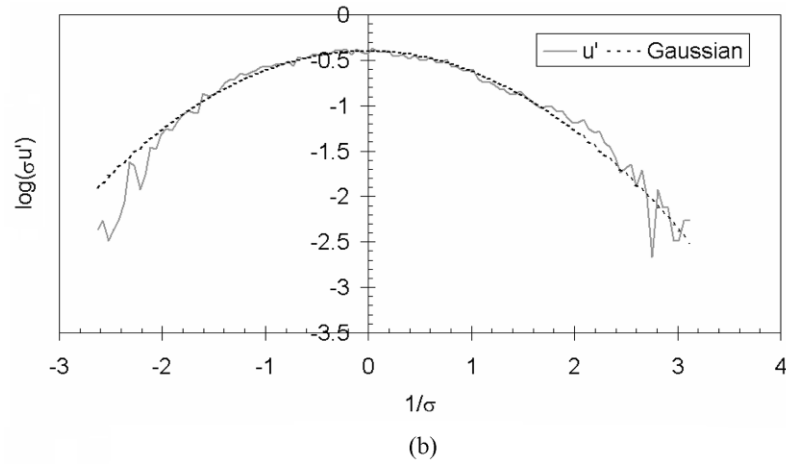
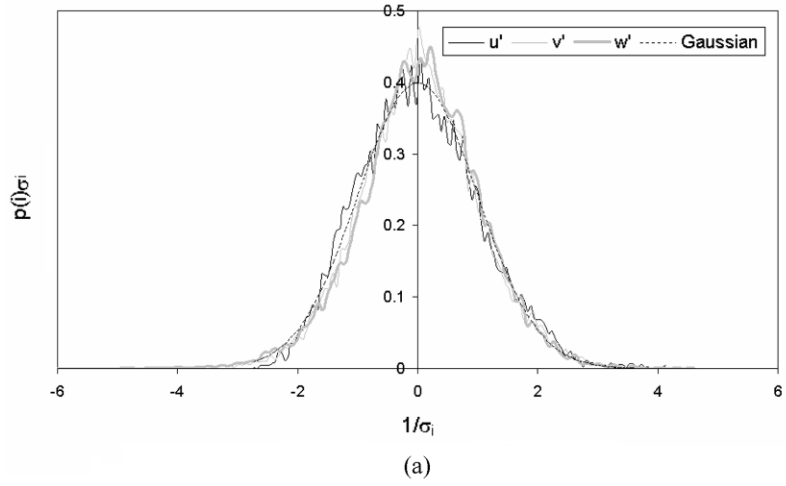


Fig. 4 (a) Probability distribution for anemometer 1, 29/04/02 data and (b) Probability distribution for  $u'$ , anemometer 1, 29/04/02 data.

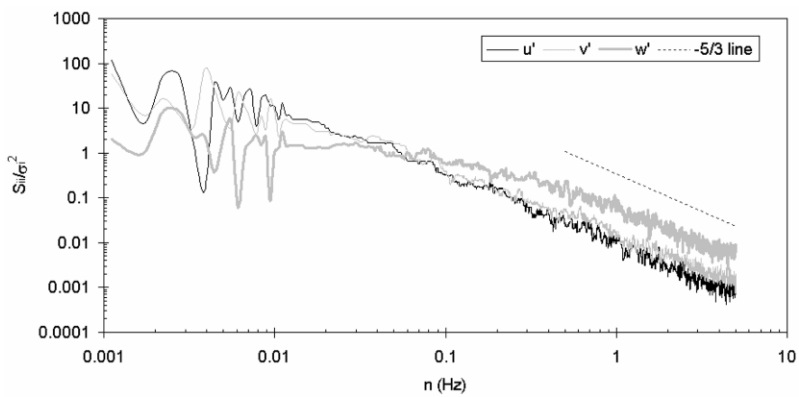


Fig. 5 Velocity power spectra for anemometer 1, 29/04/02 data

Table 3 Conventional statistical analysis of experimental pressure data

	29/04/02				14/05/02			
	1	2	3	4	1	2	3	4
I	0.116	0.121	0.121	0.142	0.076	0.076	0.067	0.079
SkewP	-0.14	-0.23	-0.28	-0.44	-0.30	-0.33	-0.23	-0.68

i.e., the slope of the curves are close to the expected  $(-5/3)$  value as illustrated in Fig. 5. This is consistent with the results of Baker (2001) and Richards, *et al.* (1997) who both analysed data from the same experiment site.

From this point onwards, unless otherwise stated all pressure data will be expressed or analysed in non-dimensionalised form with respect to the dynamic pressure, i.e.:

$$C_{pi} = \frac{P_i}{0.5\rho u^2} \quad (3)$$

where  $i = 1, 2, 3$  or  $4$  and  $P_i$  represents the calibrated pressure time series from probe  $i$ .

Table 3 shows the statistics relating to the pressure measurements.  $I$  is the standard deviation of the pressure normalised by the dynamic pressure and SkewP is the skewness of pressure. Similar to Table 2 the numbered columns in Table 3 represent the various static probes associated with the same numbered anemometers. The values of turbulence intensity have been normalised by the dynamic pressure rather than the streamwise velocity and are consistent across all probes for a particular dataset and yield reasonable values. The values of skewness are of similar orders of magnitude for each dataset with the exception of probe 4 which illustrates a consistently higher magnitude across both sets of data.

Fig. 6 shows a typical pressure spectra for all four static probes. The spectral density for each probe ( $S_{cpi}$ ) where  $i = 1, 2, 3$  or  $4$ , is divided by its variance ( $\sigma_{cpi}^2$ ) and plotted against frequency  $n$ .

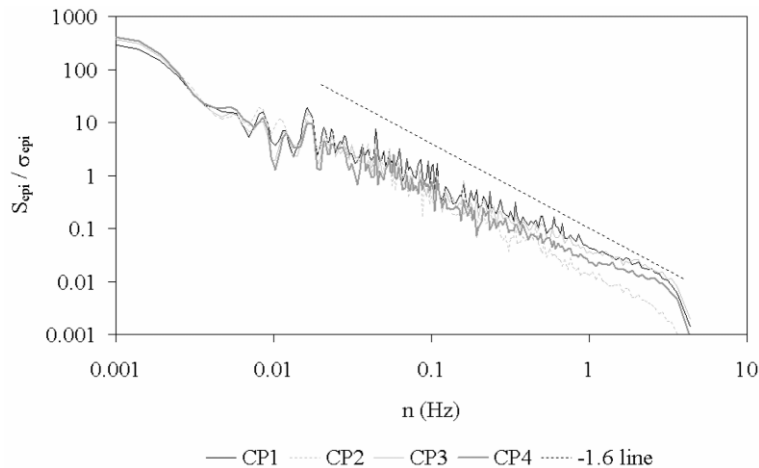


Fig. 6 Pressure power spectra for anemometer 1, 29/04/02 data

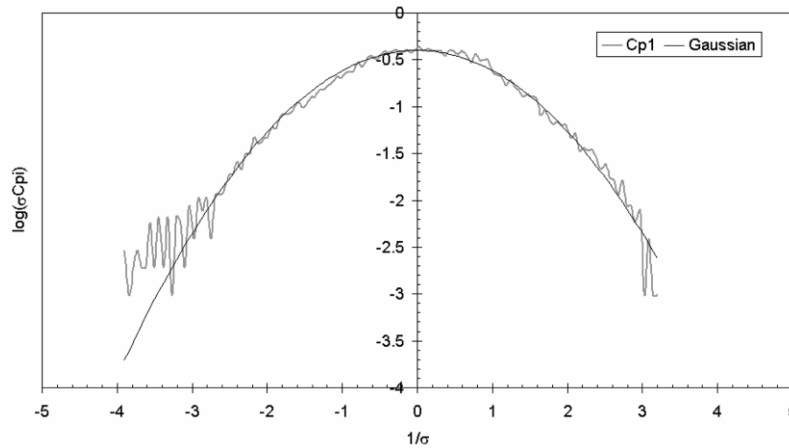


Fig. 7 Probability distribution of static pressure probe 1 on 29/04/02

A similar analysis has been undertaken for data pertaining to 14/05/02 but has not been reproduced in this paper in order to avoid repetition since the results indicated identical behaviour, i.e., all probes illustrate similar trends across the entire frequency range and the behaviour over the inertial subrange is reasonably consistent. In Fig. 6 the  $-1.6$  power law scaling appears to be a reasonable assumption and is in keeping with the findings of Elliot (1972) and Albertson, *et al.* (1998). Intuitively one would expect the pressure to scale to with  $-7/3$ , i.e., in keeping with Kolmogorov's similarity hypothesis (Kolmogorov 1941). However, the presence of the ground complicates the issue and results in large-scale pressure fluctuations arising in the outer layer of the atmospheric boundary layer straining localised pressures variations in the inner layer. This effectively leads to non-isotropic conditions and departure from the  $-7/3$  value (see Albertson, *et al.* for further details).

Fig. 7 illustrates a typical probability distribution for a static pressure probe. The data has been presented in a semi logarithmic form in order to detect any deviations from a Gaussian distribution. The deviation of the pressure from a Gaussian distribution at the lower extremes is noticeable in Fig. 7. Detailed analysis of all four static pressure probes in both datasets illustrate similar findings to those presented in Fig. 7. The results of this process have not been illustrated graphically in order to avoid the reproduction of Figures which do not significantly add to the quality of the paper. Such deviations have typically been associated with vortex motion and used to detect coherent structures (Chainais, *et al.* 1999). The reasoning behind such an association is that the corresponding high level of vorticity associated with such phenomenon results in a non-Gaussian distribution of pressure. The implications of these deviations will be examined in more detail in the following sections. However, it is perhaps worth noting that these deviations are consistent with the velocity data discussed above, since the positive values of skewness in the  $u$  component arise as a result of large fluctuations at the positive tail of the distribution. Associated with these positive fluctuations are instances of low pressure at the negative tail of the pressure distribution. These negative values of pressure result in an overall value of skewness less than zero, as evident from Table 3.

In this section the velocity and pressure results have been analysed using conventional methods and it has been demonstrated that both datasets are consistent. The analysis of pressures has revealed some interesting features. In order to examine the intermittency of flow and attempt to

Table 4 Number of extreme events occurring at each pressure probe

	29/04/02	14/05/02	Total
<i>Cp1</i>	21	28	49
<i>Cp2</i>	23	26	49
<i>Cp2</i>	22	26	48
<i>Cp4</i>	23	28	51
Total	89	108	197

understand vortex motion, a conditional analysis of both the pressure and velocity data is presented in the next section.

#### 4 Conditional analysis

Since the analysis of the pressure data in the previous section illustrated some non-Gaussian behaviour, it seems appropriate that an element of conditional analysis is also performed on this data. Full details of the technique can be found in Baker (2001), however for the purpose of clarity the method is summarised here. Firstly discrete events were identified at each static probe. These were defined as when the pressure coefficient was less than the 0.5th percentile value. ‘‘Events’’ less than two seconds apart were taken to be one event with the peak value being given by the greater value. During each event the time at which the maximum value occurred was noted. Table 4 illustrates that the number of events identified at each probe is reasonably consistent across both datasets.

In order to analyse these events in more detail the normalised pressures at a particular ‘‘trigger’’ were examined as follows. The discrete events were identified using data from a particular probe. Once the time at which an event occurred was identified, the surrounding values of normalised pressure ( $C_p$ ) for 2 seconds either side of the event were noted and used to produce a mini time series of 4 seconds worth of data zeroed on the actual event. This resulted in a number of mini time series (see Table 4) that were then ensemble averaged to produce a new time series for a particular probe. The threshold value of 0.5th percentile was chosen in order to ensure that a reasonable number of short time series were obtained, hence ensuring that the ensemble average was statistically meaningful.

The results of the conditional sampling for 14/05/02 data for different ‘‘trigger’’ probes are shown in Fig. 8. Fig. 8 illustrate a reasonably symmetric distribution for  $C_p$  with a sharp peak extending over 0.2 seconds. There are slight differences in the magnitude of  $C_p$  depending on the probe chosen, however, the general trends are sufficiently similar for the purposes of the current analysis to assume that the distribution of pressure during an event is independent of the trigger probe. This independence also held for the 29/06/02 data. Henceforth, for the entire conditional sampling, probe 1 will be used as a trigger and the conclusions drawn are assumed to be applicable to the whole of the flow.

Fig. 9 illustrates the ensemble average of the normalised pressure and normalised dynamic pressure for both datasets using probe 1 as a trigger. To aid comparison the dynamic pressure has been normalised by the average value of dynamic pressure across the whole of the dataset,  $Q$ . From Fig. 9(a) it is noticeable that although the normalised pressure data follow the same trend, the 29/

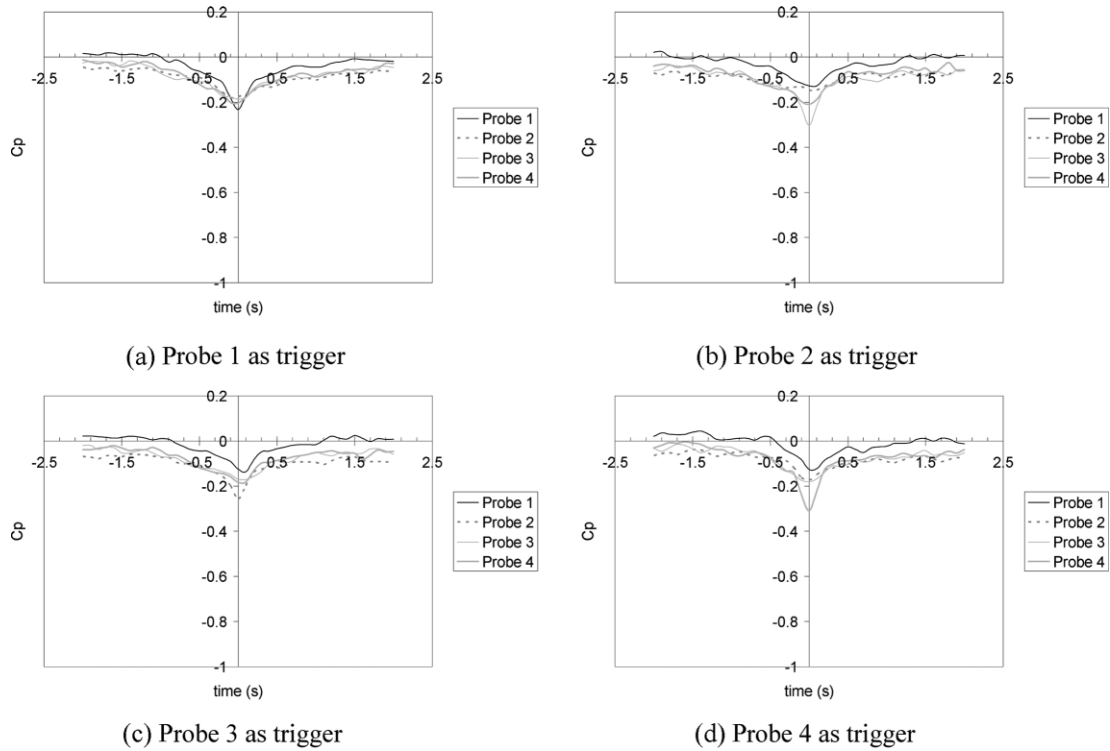


Fig. 8 99.5<sup>th</sup> percentile pressure trends for the 14/05/02 data using an event on various pressure probes as a trigger

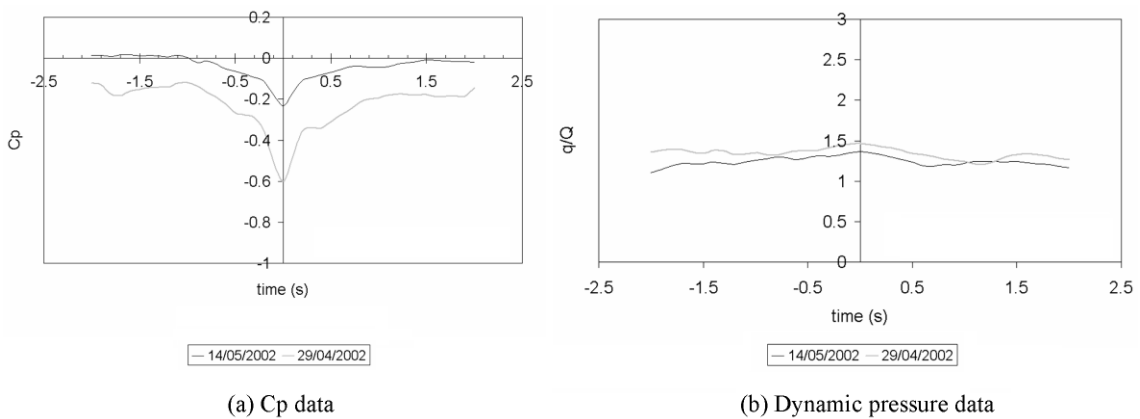


Fig. 9 Pressure and velocity ensemble averages using an event on pressure probe 1 as a trigger

04/02 dataset gives larger values of  $C_p$  across the entire dataset. The entire event also extends over the sampled time and indicates that some of the events may be associated with flow structures of a larger scale than those present in the 14/05/02 data.

In general, Fig. 9(b) illustrates that there is little noticeable difference in the behaviour of the

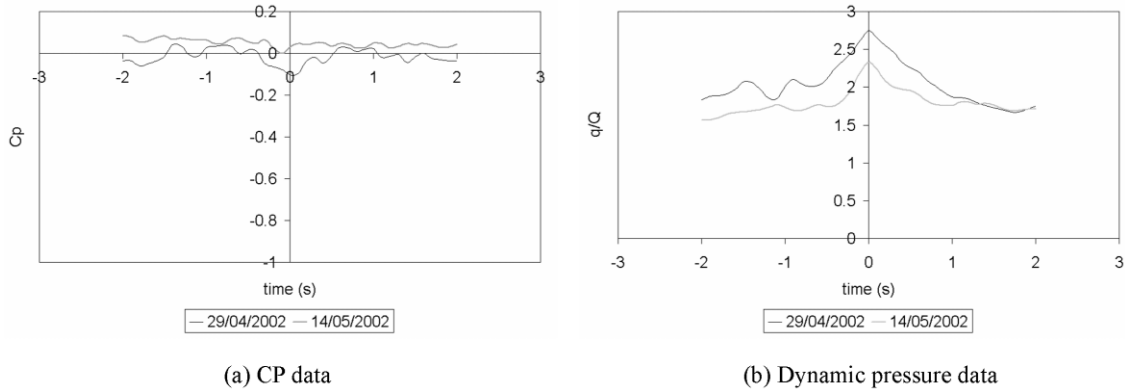


Fig. 10 Dynamic pressure used as a trigger

dynamic pressure across the whole event. The  $q/Q$  trend illustrates that the value of normalised dynamic pressure is of the order of 1.4–1.5 and suggests that the pressure events may be superimposed on large-scale velocity structures, which the anemometers effectively interpret as a slowly varying change in average velocity. It is difficult to state the exact scale of such structures since the size of the experimental ring essentially acts as a filter, however given that these events extend over a four second period and are moving with a mean velocity of the order of 7 m/s or 9 m/s (depending on dataset), then it is likely that they will be greater than 28 m or 36 m respectively. Trends in normalised velocities ( $u/U$ ,  $v/V$  and  $w/U$ ) were also investigated and illustrated no noticeable or quantifiable behaviour. This analysis is not reported since it is felt that from an engineering point of view, the relationship between pressure and dynamic pressure is of more interest, i.e., since it forms the fundamental basis of the quasi-steady relationship used in the determination of wind loading.

The trends shown in pressure in Figs. 8 and 9, i.e., the sharp peak extending over a short time period are similar to the discrete events that have been identified as present over a low-rise building (Baker 2001, Sterling, *et al.* 2003). The main difference in the findings of Sterling, *et al.* (2003) compared with the current work is that these events appear to be intensified in regions of strong vorticity, e.g., in the separation zone on the roof of a low-rise structure. If the size of the peak is related to the strength of the vortex, then Figs. 8 and 9 suggests that on average the vortex strength of the current flow is low. However, as it will be seen later this is not the case.

In addition to using the pressure at probe 1 to indicate an event, a similar analysis was undertaken using the 99.5th percentile value of the dynamic pressure data from anemometer 1 to act as a trigger (Fig. 10).

The data in Fig. 10(a) illustrates that there is little noticeable effect in the normalised pressure when the dynamic pressure is used as a trigger. Fig. 10(b) highlights that there is a rapid, localised increase in normalised dynamic pressure at the event time and that the maximum value is of the order of 2.3–2.7. Across the entire sampling period the dynamic pressure is relatively large and is fifty percent greater than the mean value. The apparent lack of correlation between the minimum pressure events and the dynamic pressure suggests that the pressure and velocity fields are essentially decoupled from each other when the dynamic pressure is a maximum, however when the pressure is a minimum (Fig. 9) there does appear to a slight correlation since  $q/Q$  values are

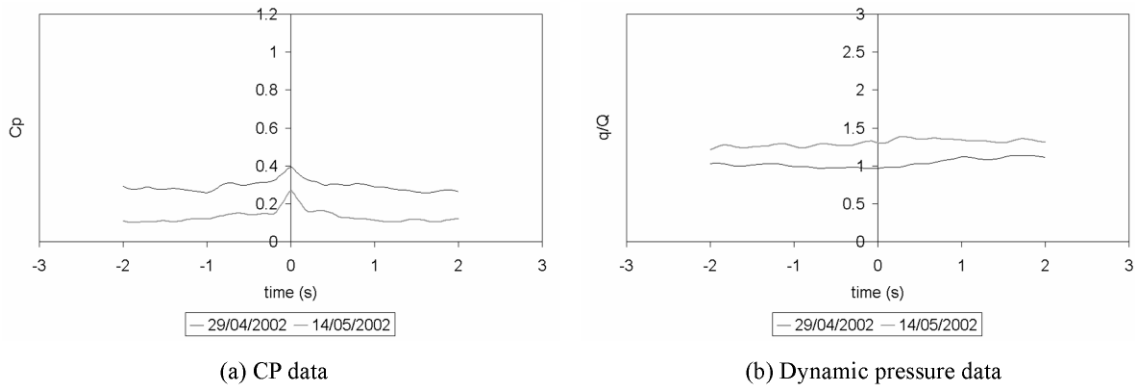


Fig. 11 Distributions of *CP* and dynamic pressure for max values of *CP*

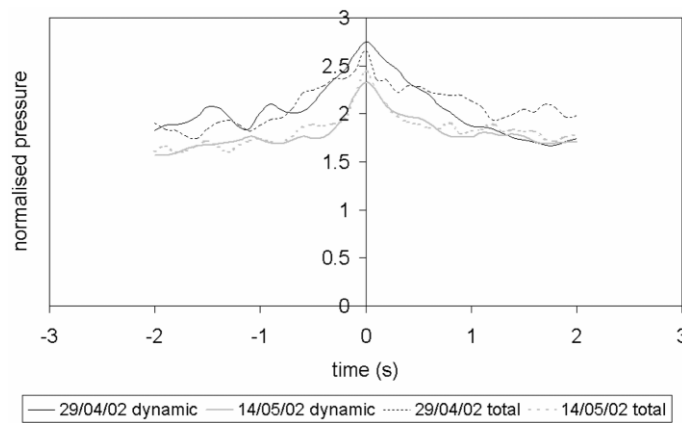


Fig. 12 Normalised total and dynamic pressure. Total pressure on sonic 1 used as a trigger

consistency greater than unity. From a loading perspective it is interesting to investigate if there is any correlation between the maximum (i.e. positive) values of pressure and dynamic pressure, since it could be envisaged that the maximum force on a windward facing wall, for example, may arise when both variables are highly correlated (this statement considers the force only on one side of the wall, since the overall force on the wall will involve a combination of other factors not least of which the pressure difference between the windward and leeward faces, see Baker (2001) for a more detailed discussion). The results of this analysis are shown in Fig. 11.

Fig. 11 illustrates similar results to Fig. 9, albeit with the negative values of Fig. 9 replaced with positive values. There is no noticeable increase in the dynamic pressure at the event time or any fluctuations over the entire sampling period. For the 29/04/02 data, the instantaneous dynamic pressure is equal to the average dynamic pressure across the entire event time. Fig. 12 shows the combined effect of total pressure (instantaneous pressure plus instantaneous dynamic pressure). The data in Fig. 12 have been normalised by the average dynamic pressure to aid in the detection of any noticeable differences between the effect of static and dynamic pressure.

The overall behaviour of the total pressure is similar to that of the dynamic pressure, indicating that dynamic pressure events are more dominant. It is interesting to note that the inclusion of the pressure terms for the 29/04/02 data is to reduce the peak in normalised pressure, whereas the opposite is true for the 14/05/02. However, these changes in peak values are relatively small and indicate that the maximum loading on the windward side of a wall, for example, is effectively dominated by the dynamic pressure and that also highlights that as with the minimum values of  $C_p$ , the maximum extreme values of  $C_p$  appear to be decoupled from the velocity field.

The analysis presented in above figures highlighted instances of an apparent decoupling between the velocity and pressure, i.e., there is evidence to suggest that extreme events arise due to the superposition of two independent mechanisms. Significant work has been undertaken in trying to elucidate vortex structures in turbulent shear flows and these methods are applied to the current data in the next section in order to examine the influence of flow structures on the pressure and dynamic pressure.

## 5. Vortex structure identification

It has long been assumed that analysing the instantaneous vorticity field will enable the presence of vortex structures to be identified. This is undoubtedly true in fully developed flows such as mixing layers, wakes and jets, where a dominant vortex scale is readily identifiable. However, in the atmospheric boundary layer the lack of a dominant eddy scale makes this process more complex. Robinson (1991) states that even instantaneous vorticity fields are inadequate to reveal coherent structures in turbulent boundary layers. Attention is often focused on identifying regions of low pressure similar to the analysis performed in Section 4, however this relies on adopting an appropriate threshold value. This threshold value may be appropriate over a small region of the flow, but as the domain increases it is likely that instances of vortex motion will pass undetected. For a thorough debate on the drawbacks of various identification methods the reader is referred to Jeong and Hussain (1995).

In an attempt to try and examine the relationship between vorticity and pressure recourse is made to the Poisson equation, which for an incompressible flow can be written as (Pope 2000):

$$-\frac{\nabla^2 P}{\rho} = \frac{\partial u_i \partial u_j}{\partial x_j \partial x_i} \quad (4)$$

Eq. (4) essentially relates the pressure field to the velocity tensor. For this equation to be valid the velocity field must remain solenoidal, (i.e., the velocity vector field is essentially divergenceless). It is possible to reduce Eq. (4) and approximate it by the first invariant of strain ( $J_1(S^2)$ ) and the first invariant of vorticity ( $J_1(\Omega^2)$ ):

$$-\frac{\nabla^2 P}{\rho} = \frac{\partial u_i \partial u_j}{\partial x_j \partial x_i} = S_{ij}S_{ji} - \Omega_{ij}\Omega_{ji} \approx J_1(S^2) + J_1(\Omega^2) \quad (5)$$

where:

$$J_1(S^2) = \left(\frac{\partial u}{\partial x}\right)^2 + \left(\frac{\partial v}{\partial y}\right)^2 + \left(\frac{\partial w}{\partial z}\right)^2 + \frac{1}{2}\left(\frac{\partial u}{\partial y} + \frac{\partial v}{\partial x}\right)^2 + \frac{1}{2}\left(\frac{\partial u}{\partial z} + \frac{\partial w}{\partial x}\right)^2 + \frac{1}{2}\left(\frac{\partial v}{\partial z} + \frac{\partial w}{\partial y}\right)^2$$

$$J_1(\Omega^2) = -\frac{1}{2}\left(\frac{\partial v}{\partial z} - \frac{\partial w}{\partial y}\right)^2 - \frac{1}{2}\left(\frac{\partial u}{\partial z} - \frac{\partial w}{\partial x}\right)^2 - \frac{1}{2}\left(\frac{\partial u}{\partial y} - \frac{\partial v}{\partial x}\right)^2 = -\frac{1}{2}\omega_x^2 - \frac{1}{2}\omega_y^2 - \frac{1}{2}\omega_z^2$$

Hence,

$$-\frac{V^2 P}{\rho} \approx \left(\frac{\partial u}{\partial x}\right)^2 + \left(\frac{\partial v}{\partial y}\right)^2 + \left(\frac{\partial w}{\partial z}\right)^2 + 2\frac{\partial u}{\partial y}\frac{\partial v}{\partial x} + 2\frac{\partial u}{\partial z}\frac{\partial w}{\partial x} + 2\frac{\partial v}{\partial z}\frac{\partial w}{\partial y} \quad (6)$$

In order to calculate the terms in Eq. (6) the data from all four anemometers were used. For the derivatives involving  $\partial y$  the velocity difference between the appropriate component of velocity from anemometers three and two were divided by the horizontal separation of the anemometers, e.g.,  $\partial v / \partial y = (v_{\text{anemometer 3}} - v_{\text{anemometer 2}}) / 1.000$ . A similar procedure was undertaken for the  $\partial z$  terms but using data from anemometers one and four. In order to calculate the  $x$  derivatives Taylor's frozen turbulence hypothesis was invoked.

Similar to the analysis presented in Section 4, once the first invariant of strain and vorticity time series had been obtained, smaller time series consisting of data from two seconds either side of the event and zeroed on the event were obtained. Table 6 represents all of the actual time of the events; the method used to identify these events are discussed more fully later. This procedure allowed

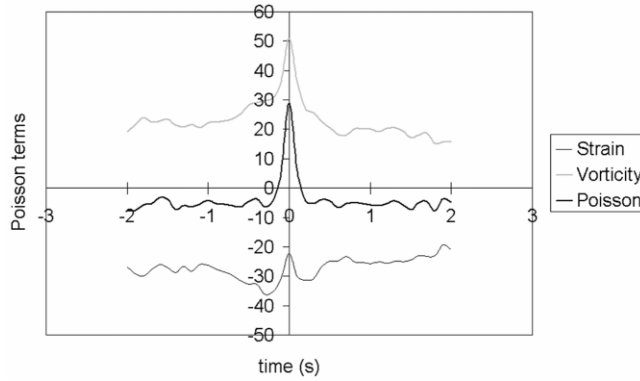


Fig. 13 Ensemble average of Poisson terms for 29/04/02 data

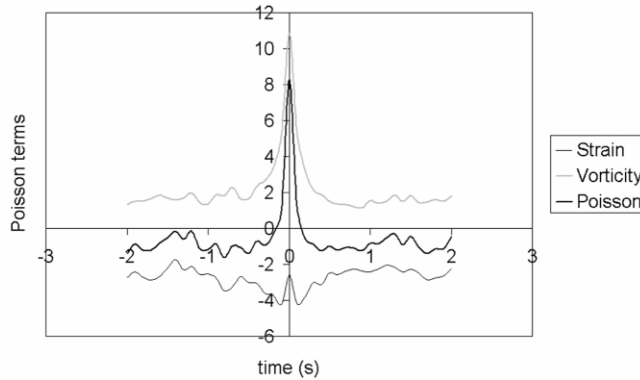


Fig. 14 Ensemble average of Poisson terms for 15/04/02 data

ensemble averages for each dataset to be obtained, the results of which are shown in Figs. 13 and 14, which clearly illustrate that in terms of the extreme events the vorticity terms dominate. In Figs. 13 and 14 the Poisson line represents the summation of the ensemble average of the instantaneous vorticity ( $J_1(\Omega^2)$ ) and strain ( $J_1(S^2)$ ) terms. There are noticeable peaks near the event time ( $t = 0$ ) for both datasets and a rapid trailing off of the pressure terms either side of the event. The peak of the events appear to be highly dependent on the data set with a maximum values of approximately  $30 \text{ s}^{-2}$  and  $10 \text{ s}^{-2}$  for the 29/04/02 and the 15/04/02 data respectively.

Although the vorticity terms dominate at the event time, not all of the changes in pressure can be solely attributed to vorticity affects. In an attempt to further investigate the relationship between changes in the pressure field and vortex structures it is necessary to identify and hence examine vortex structures within the flow. To this end resource is made to an identification method developed by Jeong and Hussain (1995). They postulate that a vortex core is a region of complex eigenvalues of the velocity gradient tensor, since complex eigenvalues imply that the local streamline pattern is closed or spiral in a reference frame moving at a point. Their technique is essentially based on the identification of a minimum pressure, but they disregard unsteady straining of the instantaneous flow field and viscous effects, both of which can lead to minimum values of pressure but without corresponding vortex motion. To understand their approach it is helpful to introduce the velocity gradient tensor:

$$\frac{\partial u_i}{\partial x_j} = S_{ij} + \Omega_{ij} \quad (7)$$

where

$$S_{ij} = \frac{1}{2} \left( \frac{\partial u_i}{\partial x_j} + \frac{\partial u_j}{\partial x_i} \right), \quad \Omega_{ij} = \frac{1}{2} \left( \frac{\partial u_i}{\partial x_j} - \frac{\partial u_j}{\partial x_i} \right) \quad (8)$$

Table 5 Percentage of the time for which  $\lambda_2$  is less than zero

	No of events	Events as a percentage of total number of data points
29/04/02	7110	39.7
14/05/02	7039	39.3

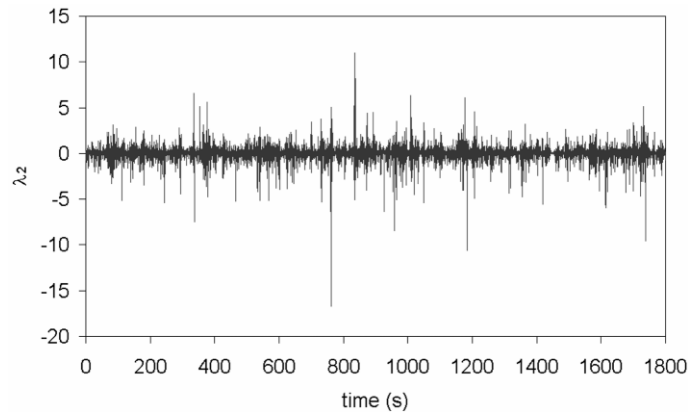


Fig. 15 Calculated time series of  $\lambda_2$  for 14/05/02

Table 6 Event time (s) for  $\lambda_2$  and conditionally sampled data ( $C_p$ ). 0.5th percentile trigger

29/04/2002				14/05/2002			
$C_p$	$\lambda_2$	$C_p$	$\lambda_2$	$C_p$	$\lambda_2$	$C_p$	$\lambda_2$
	14.1		1451.5		79		1031.2
	39.9		1456.5		111.4	1045.6	1050.2
	42.8	<b>1475.4</b>	<b>1478.5</b>		138.3	1124.8	1162.8
	67.5		1482.8		181.2		1169.5
	79.1		1494		245.1	<b>1174.1</b>	<b>1172.5</b>
	149		1496.5	<b>294.6</b>	<b>294.4</b>	1198.7	1183.7
	208.7		1501		337.4	1219.1	1206.6
	236.9		1505.4	363.9	369.6	1245.1	1257.8
	253.2	1513.8	1531.4		375.2		1313.4
	362.1	<b>1536.1</b>	<b>1536.3</b>		378.2		1317.9
	376.6	1573.9	1566.1		465.9		1353.9
	<b>373.4</b>	1596.1			532.7		1355.4
	444	1622.1			541		1358.6
371.5	642.5	<b>1624.6</b>	<b>1625.9</b>		567.7		1365.5
	693.8	<b>1632.5</b>	<b>1636.3</b>		590.7	<b>1417.8</b>	<b>1418.3</b>
	700.7	1651.2			603.2	1572	1496.7
	733.7	<b>1653.5</b>	<b>1656.7</b>	<b>624.4</b>	<b>625.7</b>	1634.7	1562.5
	737.2	<b>1683.8</b>	<b>1680.8</b>		641.4	1676.1	1594.9
	749.7		1685.9		645.3	1691.2	1614.8
	777.3	1726.8	1697.7	<b>729.5</b>	<b>731.7</b>		1618.7
	799.6	1732.4	1703.5		759.7		1676.5
	853.7	<b>1735.1</b>	<b>1734.2</b>		762.9		1688.9
	897.2	1740.1	1769.8	<b>833.4</b>	<b>834.5</b>	<b>1699</b>	<b>1698.8</b>
	900.7	1782	1786.4	<b>836.7</b>	<b>836.7</b>	<b>1721.6</b>	<b>1723.5</b>
	955.2		1793.5	859.8	871.2		1728.9
	1037.2			892.6			1736.4
	1106.6			<b>925.8</b>	<b>926.1</b>	<b>1738.8</b>	<b>1738.7</b>
1184.1	1122.8				952.6		
1302.1	1306.4				957.6		
1368.9	1375.9			<b>964.2</b>	<b>964.9</b>		
	1427.7			969.8			
<b>1431.9</b>	<b>1431.4</b>			972.7	979.6		
	1451.5			<b>981.7</b>	<b>984.1</b>		
	1456.5			984.3	994.8		
<b>1475.4</b>	<b>1478.5</b>				1010.3		
	1482.8				1020.3		

By neglecting the unsteady straining and viscous terms the method of Jeong and Hussain simplifies to finding the eigenvalues of  $S_{ij}S_{ji} + \Omega_{ij}\Omega_{ji}$ . Since  $S_{ij}S_{ji} + \Omega_{ij}\Omega_{ji}$  is symmetrical it will have three real eigenvalues ( $\lambda_1$ ,  $\lambda_2$  and  $\lambda_3$ ). Assuming that  $\lambda_1 \geq \lambda_2 \geq \lambda_3$ , then when  $\lambda_2 < 0$  the presence of a vortex will have been detected, if it is assumed that a vortex core is defined as a connected region

of two negative eigenvalues of  $\mathbf{S}^2 + \mathbf{\Omega}^2$  (Jeong and Hussain 1995). Jeong and Hussain consider that their approach is superior to other methods since their technique is not constrained to detecting results that are purely based in one plane, unlike methods that are reliant on velocity vectors (Jeong, *et al.* 1997). Table 5 and Fig. 15 illustrate the results of employing this technique to the current datasets.

Fig. 15 and Table 5 illustrate that in the current flow there is a significant presence of vortex structures of varying scale and strength. Assuming that the value of  $\lambda_2$  is indicative of the strength of the vortex then it is possible to undertake some conditional analysis and examine the effects of strong vortex motion. This assumption is consistent with the approach adopted by Jeong, *et al.* (1997) who used regions of local minima of  $-\lambda_2$  to detect coherent structures in numerically simulated flows. In keeping with the analysis presented earlier the times at which 0.5th percentile values of  $\lambda_2$  occurred were obtained. The results of this process are given in Table 6 and illustrate that the timings of the events identified with the Jeong and Hussain method do not fully coincide with the conditional sampling of the pressure data undertaken in Section 4. However, for approximately 45% of the time, the timings are sufficiently close to indicate a degree of correlation. Jeong and Hussain state that since the pressure is governed by the Poisson Eq. (6) then the pressure is inherently of a larger scale than the vorticity and as such it is problematic to identify vortex structures using solely the pressure data. This may well explain the higher level of events detected using the  $\lambda_2$  method, since this method is not solely based on identifying events which fall below a specified pressure threshold but also encompasses an identification of events based on rotational motion. Using a pressure threshold criteria will result in an under estimate of the total number of events. For example, Jeong and Hussain state "... , in general, an appropriate pressure level cannot be specified to identify all vortical regions in a flow. Also, in a mixing layer, pressure within the longitudinal ribs between large-scale spanwise rolls may not be sufficiently low, so that a single pressure threshold cannot reveal both rolls and ribs". Also as indicated earlier, the method of Jeong and Hussain is not based on identifying events that only occur in one plane, hence their approach would be expected to yield a greater number of events than one based solely on a minimum pressure threshold.

It is worth noting that the size of the experimental ring also acts as a filter and essentially restricts the size of the vortex structures that can be identified using this approach, hence it is likely that Table 6 does not represent all of the vortex structures within the flow.

It is also possible to relate the eigenvalues calculated above to the Poisson equation as follows (Jeong, *et al.* 1997):

$$-\frac{\nabla^2 P}{\rho} = \lambda_1 + \lambda_2 + \lambda_3 \quad (9)$$

The result of this process yields almost identical values to those obtained using Eq. (5) and when plotted on Figs. 13 and 14 no difference with the Poisson lines are discernable. Hence, the current dataset suggests that changes in pressure are due to either large instantaneous velocity gradients, or as a result of small scale vortex structures which in essence are decoupled from the velocity field.

Similar to the analysis undertaken in section 4, Fig. 16 illustrates the ensemble averaged normalised pressure and dynamic pressure for both datasets when the  $\lambda_2$  times are used as a trigger.

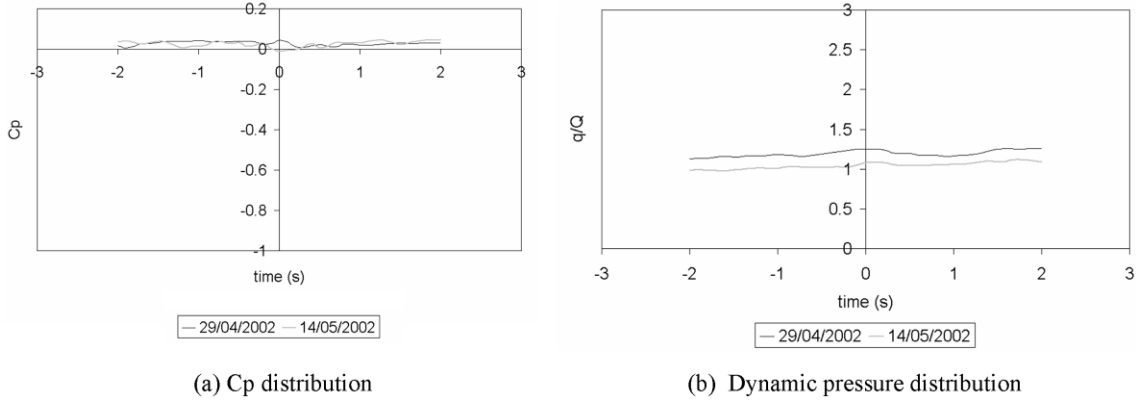


Fig. 16 Pressure and dynamic ensemble averages using  $\lambda_2$  as an event trigger

This figure clearly illustrates that there is little noticeable change in any of the time series and highlights the features demonstrated in the idealised flow case presented in Fig. 1, i.e., it is possible for a vortex to pass undetected since its imprint on the velocity field (and hence dynamic pressure) can be negligible.

## 6. Discussions and conclusions

This paper has endeavoured to examine a number of issues relating to the interaction of pressure, velocity and vortex identification in the atmospheric boundary layer. The non-stationarity of the vortex with respect to the reference frame in a real flow complicates the issue. Field tests have been undertaken and the data pertaining to two datasets with the flow normal to the experimental ring have been examined. Conventional data analysis has shown that the velocity field and corresponding statistics are as expected for flow over rural terrain. Interestingly analysis of the pressure data has shown that the distribution is non-Gaussian at the lower extreme. The analysis of the power spectra indicates a departure from Kolmogorov's  $-7/3$  scaling, however, the data is in keeping with the work of Albertson, *et al.* (1998) and arises as a result of the instantaneous pressure field being essentially non-isotropic.

Conditional sampling of the pressure field using the 0.5th percentile value of normalised pressure as a threshold, indicates a sharp, localised peak. This high intensity, rapid decrease in pressure corresponds to similar findings of the pressure coefficients over the roof of a low-rise building (Sterling, *et al.* 2003), albeit smaller in magnitude. The magnitude and trend of an event have been shown to be independent of the trigger probe for a particular dataset. However, the overall magnitude for any of the conditional sampling undertaken is consistently larger for the 29/04/02 data compared to the 14/05/02. The only significant conventional statistical difference between the two datasets is the mean velocity suggesting that the overall magnitude of the pressure fluctuations are highly related to this parameter.

For a particular pressure trigger the corresponding conditionally sampled dynamic pressure has been obtained. Analysis of this data indicates that the dynamic pressure events occur over a larger scale than the pressure and also that there is no noticeable change at or near the event

time. It is suggested that the pressure events may be superimposed on large-scale velocity structures that the anemometers effectively interpret as a slowly varying change in average velocity. It is difficult to state the scale of such structures since the size of the experimental ring essentially acts as a filter.

Conditional sampling of the pressure data using the 99.5th percentile values in order to examine the behaviour of extremes of positive pressure has been undertaken. The results show similar trends to the extreme negative pressures, i.e., a sharp peak of similar absolute value near the event time. However, one noticeable difference is that the local value of  $C_p$  either side of the pressure is reasonably constant and significantly greater than zero. This suggests that the extreme regions of positive pressure are larger in scale than their negative counter parts. An analysis of the dynamic pressure during these events (Fig. 11(b)) indicates that there is no increase in dynamic pressure across the whole of the event time that also suggests that the changes in pressure are occurring over a smaller scale than the changes in dynamic pressure.

Conditional sampling of the dynamic pressure data using the 99.5th percentile values has revealed some interesting results. Firstly that there is a large localised peak near the event time and that the minimum value of the normalised dynamic pressure across the whole of the sampling period does not fall below 1.5. These findings support those presented earlier relating to the relatively large size of such structures. The behaviour of the normalised pressure during these events is interesting and shows that there is little change over the whole of the sampling period and that the average value of  $CP$  is close to zero. These results and those when the normalised pressure is used as a trigger suggests there is a decoupling of the velocity and pressure field when an extreme event occurs.

Analysis of the normalised static pressure shows similar trends found in normalised dynamic pressure data, indicating that dynamic pressure events are more dominant. It is interesting to note that the inclusion of the pressure terms for the 29/04/02 data is to reduce the peak in normalised pressure, whereas the opposite is true for the 14/05/02. However, these changes in peak values are relatively small and indicate that the maximum loading on the windward side of a wall (for example) arises as a result of dynamic pressure.

A technique developed by Jeong and Hussain (1995) has been adopted in order to try and identify vortex structure within the flow. This technique illustrated that the flow has high occurrences of vorticity with a detection rate of 39% for both datasets. A conditional analysis was undertaken on this data in order to examine in detail the maximum values of vortex motion. The event times calculated using this method show a reasonable degree of correlation with the event times obtained from conditional sampling of the local pressure. However, they highlight the important fact that not all pressure minimum events are associated with vortex structures.

Consideration of the Poisson equation and approximation by first invariants has enabled the contribution of vorticity and straining to be examined. It has been demonstrated that the vorticity terms dominate in the generation of pressure within the flow. The Poisson equation has been expanded in terms of its first invariants and also in terms of the eigenvalues of the  $\mathbf{S}^2 + \mathbf{\Omega}^2$  matrix. The Poisson equation has also been used to demonstrate that the method proposed by Jeong and Hussain is applicable to the current flow.

Despite the relative simple geometry of the surrounding terrain, the flow has been shown to be highly unsteady and complex. The relationship between pressure, dynamic pressure and static pressure at extreme events has been investigated and the possible decoupling of the pressure and velocity field has been indicated. This combined with the high level of vorticity identified in the

flow will have important implications for structural design particularly from a serviceability perspective. More work is required at higher sampling rates in order to fully explain some of the issues raised above.

## Acknowledgements

The first author is grateful to the Nuffield foundation whose generosity through the Newly Appointed Lectures Awards programme (NUF-NAL/00674/G) made the data analysis possible.

## References

- Albertson, J.D., Katul, G.G., Parlange, M.B. and Eichinger, W.E. (1998), "Spectral scaling of static pressure fluctuations in the atmospheric surface layer: The interaction between large and small scales", *Physics of Fluids*, **10**, 1725-1732.
- Baker, C.J. (2000), "Aspects of the use of proper orthogonal decomposition in the analysis of surface pressure fields", *Wind and Struct., An Int. J.*, **3**(2), 97-115.
- Baker, C.J. (2001), "Unsteady wind loading on a wall", *Wind and Struct., An Int. J.*, **4**(5), 413-440.
- Belin, F., Maurer, J., Tabeling, P. and Willaime, H. (1996), "Observation of intense filaments in fully developed turbulence", *Journal de Physique II*, **6**, 573-583.
- Chainais, P., Abry, P. and Pinton, J.F. (1999), "Intermittency and coherent structures in a swirling flow: A wavelet analysis of joint pressure and velocity measurements", *Physics of Fluids*, **11**(11), 3524-3539.
- Elliot, J.A. (1972), "Microscale pressure fluctuations measured within the lower atmospheric boundary layer", *J. Fluid Mech.*, **53**, 351.
- ESDU (1985), Characteristics of Atmospheric Turbulence Near the Ground: Part 2 Single Point Data for Strong Wind-Neutral Atmosphere, Data Item 85020, Engineering Sciences Data Unit, London.
- Fiedler, H.E. (1988), "Coherent structures in turbulent flows", *Progress in Aerospace Sciences*, **25**(3), 231-269.
- Hussain, A.K.M.F. (1983), "Coherent structures - reality and myth", *Physical Fluids*, **26**(10), 2819-2850.
- Hussain, A.K.M.F. (1986), "Coherent structures and turbulence", *J. Fluid Mech.*, **173**, 303-356.
- Jeong, J. and Hussain, A.K.M.F. (1995), "On the identification of a vortex", *J. Fluid Mech.*, **285**, 69-94.
- Jeong, J., Hussain, F., Schoppa, W. and Kim, J. (1997), "Coherent structures near the wall in a turbulent channel flow", *J. Fluid Mech.*, **332**, 185-214.
- Kolmogorov, A.N. (1941), "The local structure of turbulence in incompressible viscous fluid for very large Reynolds numbers", *Proc. the Royal Society, London, Series A*, **434**, 9.
- Liu, J.T.C. (1989), "Coherent structures in transitional and turbulent free shear flows", *Annual Review of Fluid Mechanics*, **21**, 285-315.
- Lumley, J. and Panofsky, H. (1964), *The Structure of Atmospheric Turbulence*, Wiley-Interscience.
- Massey, B.S. (1990), *Mechanics of Fluids*, 6th Edition, Chapman and Hall Ltd, London.
- Pope, S.B. (2000), *Turbulent Flows*, Cambridge University Press, Cambridge.
- Raupach, M.R., Finnigan, J.J. and Brunet, Y. (1996), "Coherent eddies and turbulence in vegetation canopies: the mixing-layer analogy", *Boundary-Layer Meteorology*, **78**, 351-382.
- Richards, P.J., Fong, S. and Hoxey, R.P. (1997), "Anisotropic turbulence in the atmospheric surface layer", *J. Wind Eng. Ind. Aerodyn.*, **69-71**, 903-913.
- Richardson, G.M., Hoxey, R.P., Robertson, A.P. and Short, J.L. (1995), The Silsoe Structures Building: The completed experiment part 1. In *Wind Engineering Retrospect and Prospect: Papers from the 9th International Conference*, volume III. New Age International Publishers, Wiley Easton Ltd.
- Robinson, S.K. (1991), "Coherent motions in the turbulent boundary layer", *Annual Review of Fluid Mechanics*, **23**, 601-639.
- Sadani, L.K. and Kulkarni, J.R. (2000), "A study of coherent structures in the atmospheric surface layer over short and tall grass", *Boundary-Layer Meteorology*, **99**, 317-334.

Sterling, M., Baker, C.J. and Hoxey, R.P. (2003), "Short term unsteady wind loading on a low-rise building", *Wind and Struct., An Int. J.* **6**(5), 403-418.

CC